Mathematical Sciences MSc Dissertation MTHM038, 2023/24

Statistical analysis of sea turtle foraging

With an overview of Brownian motion

Daniel Marshall, 230793835

Supervisor: Dr. Rainer Klages

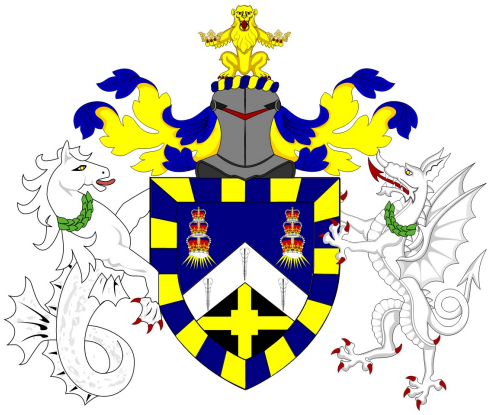

A thesis presented for the degree of

Master of Science in *Mathematics*

School of Mathematical Sciences

Queen Mary University of London

Declaration of original work

This declaration is made on September 1, 2024.

Student's Declaration: I, Daniel Cameron Marshall, hereby declare that the work in this thesis is my original work. I have not copied from any other students' work, work of mine submitted elsewhere, or from any other sources except where due reference or acknowledgement is made explicitly in the text. Furthermore, no part of this dissertation has been written for me by another person, by generative artificial intelligence (AI), or by AI-assisted technologies.
Referenced text has been flagged by:

1. Using italic fonts, **and**
2. using quotation marks "...", **and**
3. explicitly mentioning the source in the text.

Acknowledgements

I would like to thank Dr Rainer Klages for his unwavering support, encouragement and patience throughout this project. I have thoroughly enjoyed completing this project in no small part due to Dr Klages' kind and supportive approach to supervision.

I am also grateful to my current employer, Arden University, for allowing me to work on a part-time basis while carrying out this MSc in Mathematics.

Abstract

The statistical analysis of marine life foraging patterns is of contemporary significance, in view of the global pursuit to conserve oceanic biodiversity. This thesis seeks to understand sea turtle foraging patterns by applying the theory of Brownian motion to empirical data. Firstly, we explore a hierarchy of stochastic processes, ranging from the simple random walk to Langevin dynamics, in order to motivate the statistical analysis. The established theory is then applied to satellite telemetry data of three loggerhead sea turtles, foraging off the coast of West Africa. The data analysis revealed that the turtle foraging patterns do not strictly obey the theory of Brownian motion, shedding light on the complexity of animal movement.

Contents

Chapter 1

Introduction

Coherent models of animal movement allow mathematical ecologists to effectively monitor and better conserve our planet's biodiversity [Ben16]. This holds particular contemporary importance, given that climate change research has highlighted the significant impacts that complex indirect changes to an ecosystem's parameters can have on its functionality [Cah+13, Table 1].

Furthermore, this line of reasoning is also the focus of multiple international biodiversity targets [Sec01; Buc+20], signifying the global demand for sound mathematical models that monitor the dynamics of endangered species [DeA+21]. Specifically, in light of the 2015 ICUN Red List Assessment of loggerhead sea turtle endangerment [Hut17], it is imperative that the foraging models of such vulnerable marine life are routinely evaluated.

To this end, this manuscript seeks to assess whether the theory of Brownian motion is an accurate model for the foraging patterns of loggerhead sea turtles. We begin by exploring a hierarchy of stochastic processes, from the simple random walk to Langevin dynamics. Throughout the exposition of stochastic process theory in Chapter 2, we discuss important concepts to motivate the data analysis aspect of the thesis.

We then present the satellite telemetry data, collected by the Eizagurre lab [Rom22], of three loggerhead sea turtles. In Chapter 3, we illustrate the trajectories of the sea turtles and define their foraging periods. In order to motivate the next section, the speed, x-velocity, and y-velocity distributions for a single turtle are discussed and the main hypothesis is postulated: To what extent do these physical quantities adhere to the theory of Brownian motion?

Chapter 4 seeks to test this hypothesis. By plotting simple fits and quantile-quantile plots of the speed, x-velocity, and y-velocity distributions, we aim to determine the goodness of fit by these physical quantities to various relevant statistical distributions. Further analysis of the tails is conducted by plotting semi-log and log-log plots to determine whether the tails of each distribution decay as exponentials or power laws respectively. This, together with the theory established in Chapter 2, will determine the extent to which sea turtle foraging patterns obey the theory of Brownian motion.

Chapter 2

A Hierarchy of Stochastic Processes

This chapter seeks to introduce simple stochastic models of movement with the aim of applying them to describe the foraging patterns of sea turtles later in this script. Before we begin to discuss such models, we must first consider how time operates within such models. Initially, we shall refer to time being discrete, rather than continuous. It serves one to think of discrete time as snapshots of the motion as if one is generating a stop-motion animation of the motion itself [Mar11]. Moreover, another aspect which needs to be considered is the small, seemingly random, fluctuations that have been observed empirically in animal movement [Cri+92; Cus10; Goi+21]. Thus, we require a time-discretised model of movement, which incorporates randomness, to be able to model such motion. We shall now turn our attention to the fundamental mathematical theory which constitutes basic movement pattern models throughout the rest of this chapter.

2.1 Random Walks

In discretised time, the simplest approach to modelling nondeterministic motion is known as a *random walk* [KS11; CPB08].

Definition 2.1.1 (Simple Symmetric 1-D Random Walk)**.** Let $\{X_i\} \sim \text{Be}(0.5)$ for $i \in \mathbb{N}$ be a set of independent and identically distributed (i.i.d.) random variables, each taking either the value 1 or -1. Then, a simple symmetric random walk, S_n, of $n \in \mathbb{N}$ steps, is an iterative process given by

$$S_{n+1} = S_n + X_n$$

where $S_0 = 0$ denotes the initial starting point [Rév13; LL10]. See Figure A.1 in Appendix A for an illustration of a simple random walk.

One can think of S_n as a stochastic process [Doo90] that generates the position of the random walker after n steps [BW21]. Furthermore, in recognising (from Definition 2.1.1) that the individual increments of a simple random walk are independent of each other, we obtain an important and defining descriptor of a general random walk.

Definition 2.1.2 (The Markov Property for Random Walks)**.** Given a simple random walk, S_n, i.i.d increments X_i and permissible values $\{s_i\}$ for the random walk, for $i \in \mathbb{N}$, then the transition probability from step n to $n+1$ has the following property:

$$\mathbb{P}(S_{n+1} = s_{n+1} | S_n = s_n, \ldots, S_0 = s_0) = \mathbb{P}(S_{n+1} = s_{n+1} | S_n = s_n)$$

This is true for all integers j and is known as the *Markov property* or the *memorylessness property* [Dur19; AN05]).

The Markov property (see Definition 2.1.2) states that the final step taken by a random walker does not depend on the entire history of previous steps

taken. Thus, the final position travelled by the random walker (i.e., the value of S_n after n steps) becomes a topic of interest.

2.1.1 The Position Distribution

In order to examine the properties of a walker's final position, it serves us to explore its probability distribution. Figure 2.1 illustrates the evolution of the final position over an increasing number of steps, n.

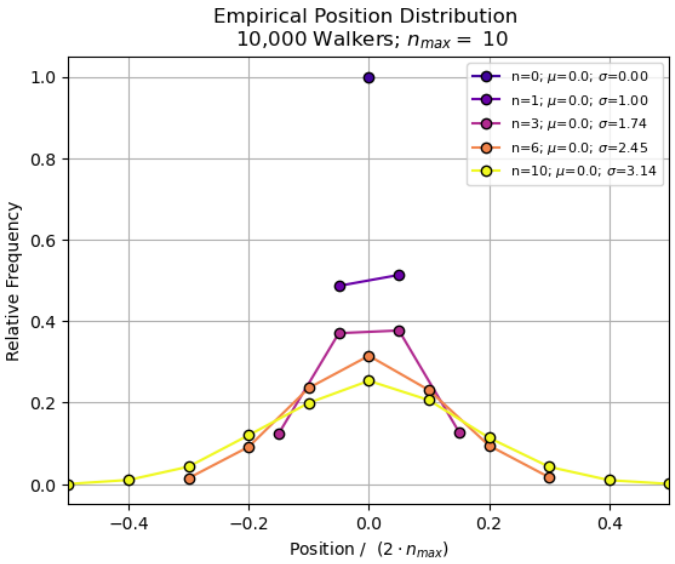

Figure 2.1: The position distribution of ten-thousand walkers after n steps. Here, μ and $\sigma(\approx \sqrt{n})$ indicate the mean and the standard deviation of the positions respectively for each n. See Appendix B for an animation of this dispersion (Self-produced in Python; see Section II of the accompanying Jupyter notebook).

Figure 2.1 infers that the position distribution converges to a Gaussian. Moreover, the standard distribution of the walker's position distribution scales as the square root of the number of steps taken [HL11]. An inter-

esting proof of this scaling for the simple random walk (i.e., $Var(S_n) \sim n$) has been provided by Milton and Ohira [MO14, pg. 392].
One can view Figure 2.1 as representing the diffusion of our random walker collective from an initial starting point over time. In the next section, we provide a rigorous definition to quantify such diffusion.

2.1.2 Mean Square Displacement

In Figure 2.1, we sample an ensemble of $N = 10000$ walkers, all starting at an initial point $x_0 = 0$, and then simulate their movement over n steps. From this, we may calculate the average square displacement, at a known time n from the initial point x_0 over the ensemble of N walkers. This is known as the *mean square displacement* [SG96, Eq. 5].

Definition 2.1.3 (Mean Square Displacement)**.** Let N be the number of random walkers, whose motion is defined in Definition 2.1.1, in an ensemble where the displacement of the i-th walker at a given time n is denoted as $x^{(i)}(n)$. Then, the average square displacement, at a given time n, over the N-walker ensemble, is known as the *mean square displacement* [SG96]:

$$\text{MSD}(n) \equiv \frac{1}{N} \sum_{i=1}^{N} \left[x^{(i)}(n) - x^{(i)}(0)\right]^2$$

2.1.3 Central Limit Theorem for the Simple Random Walk

In order to model movement more precisely, we should consider models in continuous space. To achieve this transition from discrete space to continuous space, we can apply the following theorem:

Theorem 2.1.4 (Central Limit Theorem for Random Walks)**.** *Let S_n be a random walk, as defined in Definition 2.1.1, then*

$$\frac{S_n}{\sqrt{n}} \xrightarrow{d} \mathcal{N}(0,1) \text{ for } n \to \infty$$

This is known as the Central Limit Theorem for simple random walks ([HL13, Eq. B.10 - B.12, pg. 445 - 448]; [LL10, pg. 24]).

One can infer from this that the position of a random walker, in a large-step limit, converges to that of the standard Gaussian and is continuous in space. Interestingly, Reif [Rei09, pg. 17-21] uses Taylor Expansions to justify space-continuity in this limit, as an alternative to the Central Limit Theorem.
Though Theorem 2.1.4 allows for a space-continuous model of animal movement, we are still reliant on discretised time. Therefore, it stands to reason that we may wish to evaluate the movement in continuous time $t \in \mathbb{R}_{\geq 0}$, allowing for continuity to be modelled and to provide a more accurate reflection of real-world sea turtle swimming patterns [Aba+23, Fig. 2]. The below theorem ensures such time-continuity.

Theorem 2.1.5 (Donsker's Theorem)**.** *In the large step limit, the rescaled random walk, $W^{(n)}(t)$, defined by*

$$W^{(n)}(t) := \frac{S_{\lfloor nt \rfloor}}{\sqrt{n}}$$

converges in distribution to a Gaussian of mean zero and variance t for some $t \in [0,1]$. That is to say,

$$\frac{S_{\lfloor nt \rfloor}}{\sqrt{n}} \xrightarrow{d} \mathcal{N}(0,t) \text{ as } n \to \infty$$

This is known as Donsker's Invariance Principle [Don52].

In taking the large-step limit and utilising Donsker's Invariance Principle (Theorem 2.1.5), which generalises the Central Limit Theorem (Theorem 2.1.4), we have arrived at space- and time-continuous approach to modelling animal movement.

2.2 Wiener Process

As a natural extension of the large-step limit random walk combined with Donsker's Invariance Principle, the Wiener process is a stochastic process which models movement in continuous space and time [Csö79].

Definition 2.2.1. (Wiener Process) The Wiener Process, $W(t)$, is a stochastic process which is governed by the following equation of motion:

$$dW(t) = \xi(t)\, dt$$

where $\xi(t)$ is a value sampled from $\mathcal{N}(0, t)$. Moreover, the Wiener Process satisfies the following properties [Dur19; LK19]:

1. The process starts at zero (i.e., $W(0) = 0$)
2. The increments of W are independent (i.e., for some $t, \epsilon > 0$, $W(t+\epsilon) - W(t)$ is independent of all past values $W(s)$ for $s < t$).
3. Each increment is normally distributed with zero mean and variance equal to the time interval of the increment (i.e., $W(t+\epsilon) - W(t) \sim \mathcal{N}(0, \epsilon)$).
4. $W(t)$ is continuous on t.

Please see Figure A.2 for a simulation of a Wiener process.

Notice that we have now dropped the n steps as this process is now in continuous time, $t \in \mathbb{R}_{\geq 0}$, rather than discrete time, $n \in \mathbb{N}$. One should also recognise that the Wiener Process is essentially a time-continuous random walk with Gaussian-distributed increments. One may wish to verify that the third property of Definition 2.2.1 holds by realising that the Normal distribution is closed under the subtraction of two normally distributed random variables [Lem02, Eq. 5.2.1].

2.3 Ornstein-Uhlenbeck Process

Despite the continuity in time and space, the Wiener process does not exhibit a precise, smooth approach to modelling movement. Specifically, the Wiener process is non-differentiable everywhere [LK19], meaning that one cannot explicitly derive velocities from a Wiener process. Therefore, we require a Gauss-Markov [RW05] stochastic process which admits a stationary velocity distribution [Ros10]. Such a process is known as the Ornstein-Uhlenbeck process.

Definition 2.3.1. (Ornstein-Uhlenbeck Process) The Ornstein-Uhlenbeck Process, $U(t)$, is a stochastic process given by the following stochastic differential equation [Øks98]:

$$dU(t) = \theta[\mu - U(t)]\,dt + \sigma\,dW(t)$$

where $\mu > 0$ is the mean value of the process, $\theta > 0$ is the rate of mean reversion (i.e., the rate at which the process is likely to return to its mean value), and σ is the standard deviation (per square root time) of the random noise described by the Wiener process, $W(t)$ [Jac96].
Consequentially, the Ornstein-Uhlenbeck process, $U(t)$, satisfies the following properties:

1. $U(t)$ is stationary. This means it admits a distribution that does not explicitly depend on time.
2. $U(t)$ is a Markov process (see Definition 2.1.2).
3. $U(t)$ is a Gauss process; its randomness is determined by a Gaussian distribution.

See Figure A.3 for a simulation of an Ornstein-Uhlenbeck process.

2.4 Langevin Dynamics and Brownian Motion

Langevin dynamics is a theory of particle movement which considers the forces applied to a particle traversing in a viscous fluid [ST19]. Specifically, Langevin accounts for both the deterministic friction force acting on the particle, as a result of the fluid's viscosity, and the forces arising from the numerous collisions of much lighter particles suspended in the fluid (see Figure C.1) [Con+21]. Such motion is known as Brownian motion [Has16]. This allows us to model the noise which is inherent in the particle's movement, whilst acknowledging the deterministic friction force exerted on the particle [CKW04].

Definition 2.4.1. (Langevin Equation of Motion) Let $x(t)$ be the position of a particle and let $v(t) = \mathrm{d}x(t)/\mathrm{d}t$ define its velocity. Then, the Langevin equation of motion is given by:

$$m\frac{\mathrm{d}v(t)}{\mathrm{d}t} = -\lambda v(t) + \xi(t)$$

where m is the mass of the particle, λ is a damping coefficient, and $\xi(t)$ is the time-derivative of an interpolation of the Wiener process,

$W(t)$ ([Con+21]; see also [LG97]). Please see Appendix C for a physical derivation using elementary mechanics.

One should note that the Wiener process is a fundamental aspect of Brownian motion, as it encapsulates the randomness that is observed from molecular collisions [LG97]. Physicists refer to the Langevin equation as a holistic picture of Brownian motion, whereas mathematicians cite the Wiener process as Brownian motion [Has16].

The link between Wiener processes and Langevin dynamics can be observed when one takes the overdamped limit. That is, the limit when the colliding particles are microns in diameter, the Reynold's number [GW14] of the viscous flow is negligible, and consequentially has minimal contribution to the inertial force (i.e., $\mathrm{d}v_t/\mathrm{d}t \approx 0$) [Mar99]. In this limit, the Langevin equation, as defined in Definition 2.4.1, becomes

$$\begin{aligned} 0 &= -\lambda v(t) + \xi(t) \\ \Rightarrow v(t) &= \frac{1}{\lambda}\xi(t) \end{aligned}$$

Essentially, this means that, when the force due to the particle's acceleration is negligible, one returns to motion modelled by the Wiener process.

2.4.1 Velocity Probability Distribution Function

It is important to consider the probability distribution function of the particle's velocity as statistical models enable one to understand movement.
Firstly, we recognise that the velocity distribution must be of Gaussian form, due to the linearity of the Gaussian distribution together with the fact that the Langevin equation (see Definition 2.4.1) contains the Wiener 'Gaussian noise' term. Therefore, to find the velocity probability distribution function in full detail, one must find the defining features of the Gaussian distribution (i.e., its mean and variance) [Lyo14]. To do this, we must solve the Langevin

equation to find the velocity.

$$m\frac{\mathrm{d}v(t)}{\mathrm{d}t} = -\lambda v(t) + \xi(t) \tag{2.1}$$

Here, we shall use the integrating factor approach [Ada02], which means multiplying Equation 2.1 by the integrating factor, $e^{\lambda t/m}$:

$$e^{\lambda t/m} m\frac{\mathrm{d}v(t)}{\mathrm{d}t} = -\lambda e^{\lambda t/m} v(t) + e^{\lambda t/m}\xi(t) \tag{2.2}$$

Simplifying Equation 2.2, and applying the product rule, we obtain:

$$\begin{aligned} e^{\lambda t/m} m\frac{\mathrm{d}v(t)}{\mathrm{d}t} + \lambda e^{\lambda t/m} v(t) &= e^{\lambda t/m}\xi(t) \\ \Rightarrow \quad \frac{\mathrm{d}}{\mathrm{d}t}\left(m e^{\lambda t/m} v(t)\right) &= e^{\lambda t/m}\xi(t) \end{aligned} \tag{2.3}$$

Now, we shall integrate both sides of Equation 2.3 with respect to t, using the dummy variable s:

$$\begin{aligned} \int_0^t \frac{\mathrm{d}}{\mathrm{d}s}\left(m e^{\lambda s/m} v(s)\right)\mathrm{d}s &= \int_0^t e^{\lambda s/m}\xi(s)\mathrm{d}s \\ \Rightarrow \quad m e^{\lambda t/m} v(t) - m v(0) &= \int_0^t e^{\lambda s/m}\xi(s)\mathrm{d}s \end{aligned} \tag{2.4}$$

Dividing both sides of Equation 2.4 by $me^{\lambda t/m}$, and making $v(t)$ the subject, gives [Sjo09]:

$$v(t) = v(0)e^{-\lambda t/m} + \frac{1}{m}\int_0^t e^{-\lambda(t-s)/m}\xi(s)\mathrm{d}s \tag{2.5}$$

From Equation 2.5, together with the linearity of the expectation operator and that $\mathbb{E}[\xi(t)]$ is zero for all $t \in \mathbb{R}$, we can recognise that the expectation of $v(t)$ is given by

$$\mathbb{E}[v(t)] = v(0)e^{-\lambda t/m} \tag{2.6}$$

Moreover, it can be shown that the variance of $v(t)$ can be written as [Cro23]:

$$\mathrm{Var}(v(t)) = \frac{k_B T}{m}\left(1 - e^{-2\lambda t/m}\right) \tag{2.7}$$

where k_B is Boltzmann's constant and T is the temperature of the system [Cro23]. Therefore, the velocity probability distribution function, $P(v,t)$, is given by:

$$P(v,t) = \sqrt{\frac{m}{2\pi k_B T(1 - e^{-2\lambda t/m})}} \exp\left(-\frac{m(v - v(0)e^{-\lambda t/m})^2}{2k_B T(1 - e^{-2\lambda t/m})}\right) \tag{2.8}$$

2.4.2 Deriving the Mean Square Displacement Using the Langevin Equation

We may recall from Definition 2.1.3 that the mean square displacement measures the average squared displacement of a moving object and is an important descriptor for the dispersion of said particle. In this section, we derive the mean square displacement using the Langevin equation (see Definition 2.4.1), replicating the proof found in Cross [Cro04].

Before we begin, we must first acknowledge the following identities. Given a smooth position function $x(t)$ and a smooth velocity function $v(t) := \mathrm{d}x/\mathrm{d}t$, Identity 2.9 and Identity 2.10 hold:

$$xv \equiv x\frac{\mathrm{d}x}{\mathrm{d}t} \equiv \frac{1}{2}\frac{\mathrm{d}x^2}{\mathrm{d}t} \tag{2.9}$$

$$x\frac{\mathrm{d}v}{\mathrm{d}t} \equiv \frac{1}{2}\frac{\mathrm{d}^2x^2}{\mathrm{d}t^2} - v^2 \tag{2.10}$$

We start by multiplying the Langevin equation (see Equation 2.1) by x, dropping the explicit dependencies of x, ξ, and v on t for clarity:

$$xm\frac{\mathrm{d}v}{\mathrm{d}t} = -x\lambda v + x\xi \tag{2.11}$$

Recognising that $v = \mathrm{d}x/\mathrm{d}t$, we rewrite Equation 2.11 using first and second-order derivatives of x:

$$xm\frac{\mathrm{d}^2x}{\mathrm{d}t^2} = -x\lambda\frac{\mathrm{d}x}{\mathrm{d}t} + x\xi \tag{2.12}$$

This enables us to use Identity 2.9 and Identity 2.10 to rewrite this in terms of derivatives of x^2.

$$m\left(\frac{1}{2}\frac{\mathrm{d}^2x^2}{\mathrm{d}t^2} - v^2\right) = -\frac{\lambda}{2}\frac{\mathrm{d}x^2}{\mathrm{d}t} + x\xi \tag{2.13}$$

One may consider the averages of these variables, recognising that $\langle\xi\rangle$ vanishes for all $t \in \mathbb{R}$ and that the noise term is uncorrelated with the position [Cro04]:

$$m\left(\frac{1}{2}\frac{\mathrm{d}^2\langle x^2\rangle}{\mathrm{d}t^2} - \langle v^2\rangle\right) = -\frac{\lambda}{2}\frac{\mathrm{d}\langle x^2\rangle}{\mathrm{d}t} \tag{2.14}$$

Now, one can rewrite this in the general form of an inhomogeneous differential equation. Furthermore, one can evaluate $\langle v^2\rangle$, with respect to the large-time limit, in accordance with Equations 2.6 and 2.7.

$$\frac{\mathrm{d}^2\langle x^2\rangle}{\mathrm{d}t^2} + \frac{\lambda}{m}\frac{\mathrm{d}\langle x^2\rangle}{\mathrm{d}t} = \frac{2k_BT}{m} \tag{2.15}$$

To solve this inhomogeneous differential equation for $\langle x^2\rangle$, one must first solve the homogeneous equation [Rob04]. Its solution is given by Equation 2.16, where the real constants c_1 ad c_2 are yet to be determined.

$$\langle x^2\rangle = c_1 + c_2e^{-\frac{\lambda}{m}t} \tag{2.16}$$

Furthermore, we must find a particular solution of the inhomogeneous differential equation. The ansatz for the particular solution is chosen to be

$$\langle x^2\rangle = At \tag{2.17}$$

Now, we shall substitute the particular solution into the differential equation (Equation 2.15) to be able to evaluate A.

$$\frac{\mathrm{d}^2(At)}{\mathrm{d}t^2} + \frac{\lambda}{m}\frac{\mathrm{d}(At)}{\mathrm{d}t} = \frac{2k_BT}{m}$$

$$\Rightarrow \; 0 + \frac{\lambda}{m}A = \frac{2k_BT}{m}$$

$$\Rightarrow \; A = \frac{2k_BT}{\lambda} \tag{2.18}$$

By combining the particular solution (2.17) and the solution to the homogeneous differential equation (2.16), we obtain the following general solution:

$$\left\langle x^2 \right\rangle = c_1 + c_2 e^{-\frac{\lambda}{m}t} + \frac{2k_BT}{\lambda}t \tag{2.19}$$

In order to find the constants c_1 and c_2, one may use the initial conditions of the system:

$$x(0) = 0 \quad \text{and} \quad \left.\frac{dx}{dt}\right|_{t=0} = 0 \tag{2.20}$$

This provides the following solution to the inhomogeneous differential equation:

$$\left\langle x^2 \right\rangle = -\frac{2k_BTm}{\lambda^2} + \frac{2k_BTm}{\lambda^2}e^{-\frac{\lambda}{m}t} + \frac{2k_BT}{\lambda}t \tag{2.21}$$

Equation 2.21 illustrates the long-time rate of dispersion which we identified in Section 2.1.1. More precisely, according to the theory of Brownian motion, as t becomes sufficiently large, the mean square displacement grows linearly (i.e., $\langle x^2 \rangle \sim t$) [KSZ96].

Chapter 3

Presenting and Processing the Empirical Data

We shall now focus our attention to the analysis of sea turtle swimming patterns, inspired by the theory we have discussed throughout Chapter 2. The data, courtesy of the Eizagurre lab [Rom22], contains geolocation information on loggerhead sea turtle movement patterns off the coast of West Africa (see Figure 3.1). Loggerhead sea turtles utilise the Cabo Verde archipelago as a nesting site and the eastward stretch of the Atlantic Ocean as foraging grounds [Pat+22]. We seek to analyse satellite telemetry data to understand their movement patterns when foraging.

3.1 Dataset Overview

To begin this chapter, we shall explore the trajectories of three sea turtles: Lola, Manou, and Speedy. The data has been collected between 20 August 2021 and 22 June 2022. Figure 3.1 shows the raw data for Speedy in a tabulated format. The raw data contains the following headers:

- **Date** shows the timestamp of when the position was measured and recorded by the satellite.

- **Type** denotes the satellite that recorded the data. In this dataset, we have the Argos satellite [Arg24] and the FastGPS satellite recording the trajectories of the turtles.
- **Quality** informs the reader of the quality of the measurement, taking values in the set 7, 6, 5, 4, 3, 2, 1, 0, A, B, Z. The highest quality data points are marked 7, whereas the lowest quality data points are marked Z.
- **Latitude** denotes the North-South angular position of an object on the Earth's surface, either above or below the equator, measured in degrees [Saj08].
- **Longitude** is defined as the East-West position of an object on the Earth's surface relative to the Prime Meridian [Saj08].

Date	Type	Quality	Latitude	Longitude
12:11:17 20-Aug-2021	Argos	3	16.6200	-22.9240
19:41:01 26-Aug-2021	Argos	3	16.6189	-22.9241
19:41:01 26-Aug-2021	Argos	3	16.6189	-22.9241
20:50:04.975312 26-Aug-2021	FastGPS	4	16.6172	-22.9189
20:52:04.998125 26-Aug-2021	FastGPS	5	16.6146	-22.9136
...	...	...	...	...
11:31:47 29-Apr-2022	Argos	3	10.3550	-18.6470

Figure 3.1: Raw data for the trajectory of Speedy. The raw data for Lola and Manou follow the same frame.

In order to mitigate the impact of measurement error on the imprecision of the turtle trajectories, we have filtered all of the data points that have a quality index greater than '0' which was decided via a purely visual approach. However, it is important to note that this has limited the number of data points available for analysis (see Figure 3.2). In the next section, we shall explore the trajectories of the three turtles.

Quality	Lola	Manou	Speedy
All	4082	3713	3705
>A	2835	2268	2443
>0	2157	1682	1965

Figure 3.2: The number of data points for each turtle after specific quality filters have been applied.

3.2 Latitude-Longitude Plot

Initially, we observe the latitude-longitude plot seen in Figure 3.3. The turtles begin their journey on the southeastern coast of Sal and make their way foraging through the North Atlantic Ocean. For the purposes of this analysis, we claim that the foraging period commences for each turtle after its first sharp turn.

A latitude-longitude plot of the turtles' trajectories during this foraging period can be found in Figure D.1. One may notice that this movement is atypical of Brownian motion; the large loops in Lola's trajectory suggest that the movement is determined by its own intrinsic needs when foraging. Moreover, Figure E.1 demonstrates Speedy's autonomy in this regard; the apparent fluctuation in speed throughout its trajectory indicates that its movement is influenced by extraneous factors that are not considered by the theory of Brownian motion.

Throughout the remainder of this chapter, we shall explore the distributions of the turtles' speeds, x-velocities, and y-velocities to determine how close this empirical data is congruent with the theory of Brownian motion.

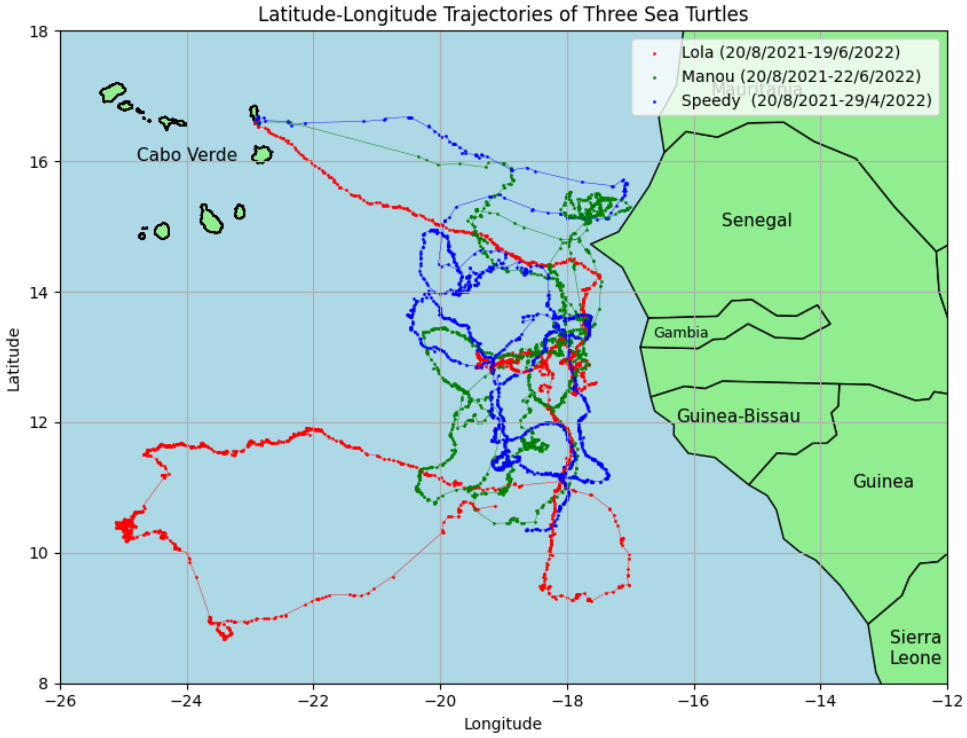

Figure 3.3: The latitude-longitude plot for Lola, Manou, and Speedy. Before plotting, the data had been filtered for those points with a quality greater than '0' (self-produced using Python; see Sections III and IV).

3.3 Cleaning the Data

The analysis of the cleaned data will only concern the foraging period of Speedy. Moreover, one must recognise the temporal noise that exists within the GPS recordings; the time between data points fluctuates significantly. As such, we consider removing the clusters of points which have a notably longer time difference between their recordings. On the other hand, we also have data points which are mere seconds apart, often indicating a double recording by the GPS receiver. Thus, we must eliminate those points in our cleaned data. To do this, one can calculate the time difference between each

Speedy recording and illustrate them on a boxplot (see Figure 3.4). In order

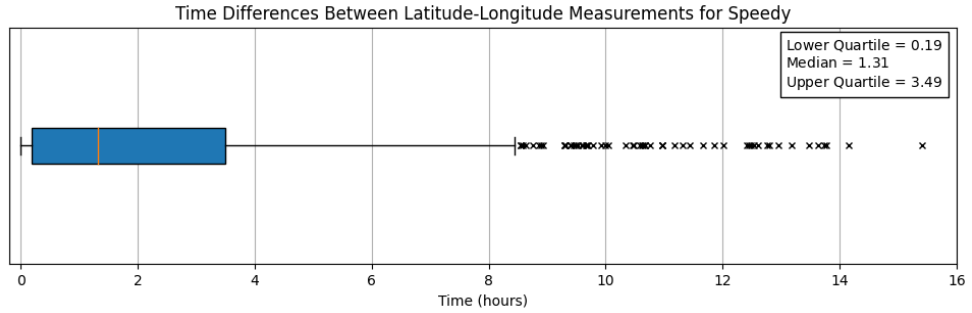

Figure 3.4: A boxplot of time differences in the GPS recordings of Speedy's position (self-produced using Python; see Sections III and VI).

to extract those data points that are chronologically sensible, we remove clusters of points that have a time difference less than three minutes apart and those clusters that have a time difference beyond the 95%-quantile.
The above restriction on time differences between clusters form the definition of our cleaned data. In the next section, we shall utilise linear interpolation to estimate additional data points.

3.4 Interpolating the Data

Linear interpolation allows data scientists to construct additional data points within a dataset by assuming that there is a linear relationship between consecutive data points. Figure 3.5 demonstrates the mechanics of linear interpolation. For the purposes of this manuscript, linear interpolation enables one to effectively pad out the trajectory, introducing new points that somewhat fit the turtles' movement patterns.

To interpolate the data, we utilised the Numpy interp method to pad out the longitude and latitude datasets for Speedy with a constant time step of

the median time difference (see Figure 3.4). This enables us to retrieve an interpolated dataset of lat-long points which are 1.31 hours apart for the raw data and 1.87 hours apart for the cleaned data.

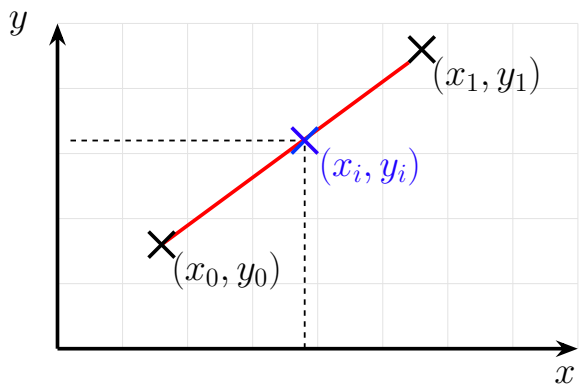

Figure 3.5: A diagram illustrating the mechanics of linear interpolation. One assumes that any two consecutive points, say (x_0, y_0) and (x_1, y_1), are linearly related. Consequentially, one may insert a point, (x_i, y_i), on the line in between two known points to effectively pad out the dataset (self-produced, using TikZ).

3.5 Speed, x-Velocity, and y-Velocity Distributions

This section will examine the speed, x-velocity, and y-velocity distributions of Speedy's trajectory. One may postulate, from Figure 3.6, that the cleaning and interpolating of the data allows the speed and velocity distributions to take the form of Rayleigh and Gaussian distributions respectively. Moreover, one would expect the velocities to take Gaussian form, given the derivation provided in Section 2.4.1. However, attaining a Rayleigh distribution for the speed is less trivial. Given an x-velocity Gaussian variable, v_x, and

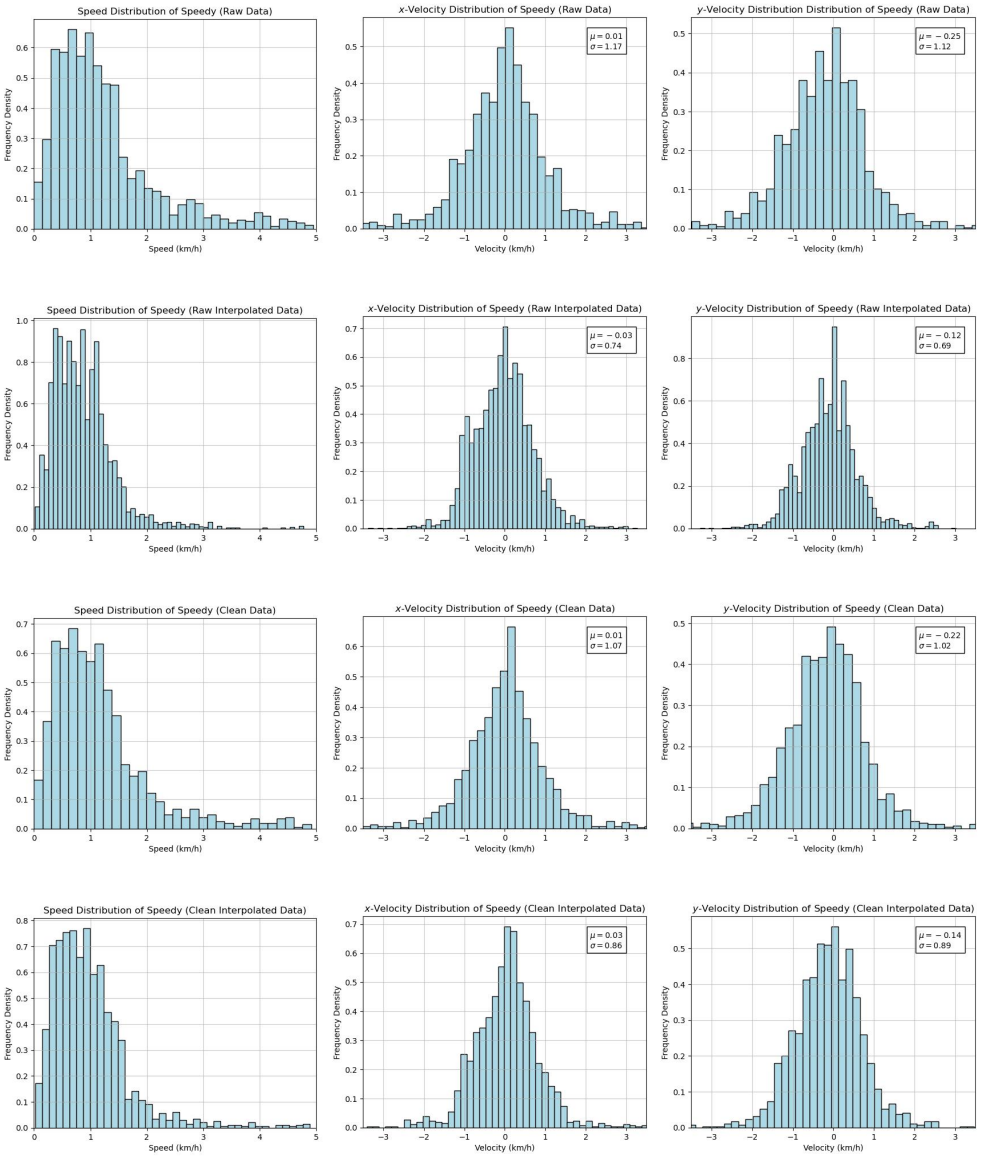

Figure 3.6: The speed, x-velocity, and y-velocity distributions for the raw Speedy data, the raw interpolated Speedy data, the clean Speedy data, and the clean interpolated Speedy data (self-produced using Python; see Sections III-IX of the accompanying Jupyter notebook).

a y-velocity Gaussian variable, v_y, one can define their joint distribution, $\rho(v_x, v_y)$, since v_x and v_y are independent, in the following way:

$$\rho(v_x, v_y) \sim e^{-(v_x^2+v_y^2)}$$

One can then transform this joint distribution into polar coordinates (i.e., $\rho(v_x, v_y) \leftrightarrow \rho(v, \varphi)$, where v is the speed variable and φ is the angle of movement). Recall from undergraduate algebra courses, we require the introduction of the Jacobian determinant to satisfy the equality when changing variables [Kap91]. Given the standard change of variables from Cartesian to polar coordinates:

$$v_x = v\cos\varphi \quad \text{and} \quad v_y = v\sin\varphi$$

The determinant of the Jacobian, J, can be calculated as follows:

$$|J| = \begin{vmatrix} \frac{\partial v_x}{\partial v} & \frac{\partial v_x}{\partial \varphi} \\ \frac{\partial v_y}{\partial v} & \frac{\partial v_y}{\partial \varphi} \end{vmatrix} = \begin{vmatrix} \cos\varphi & -v\sin\varphi \\ \sin\varphi & v\cos\varphi \end{vmatrix} = v\cos^2\varphi + v\sin^2\varphi = v$$

Thus, applying the change of variables to the probability distribution yields the following result:

$$\begin{aligned} \rho(v, \varphi) &= \rho(v_x, v_y)\,|J| \\ \Rightarrow \rho(v, \varphi) &\sim ve^{-v^2} \end{aligned}$$

Therefore, the distribution of the two-dimensional speed random variable, given Gaussian x- and y-velocities, can be defined as a Rayleigh distribution [CS21].

From Figure 3.6, we observe that the distribution of the speed begins to take the form of a Rayleigh distribution. Interpolation of the raw speed data highlights the non-uniform time density of the data points; the large variance

of time differences observed in the raw data leads to inaccurate interpolation.

Furthermore, the above point highlights the importance of cleaning the data. One can notice that, after cleaning (see Section 3.3), the speed distribution is adopting a clearer Rayleigh-like functional form. Interpolating the clean data, as discussed in Section 3.4, enables this Rayleigh-like shape to become more evident.

We further observe the benefits of cleaning and interpolating the data within the progression of the x-velocities and y-velocities. The data processing further illustrates the Gaussian-like form of the velocity distributions.

In the next chapter, we will investigate to what extent the movement of Speedy fits the theory of Brownian motion.

Chapter 4

Testing Data Consistency with Brownian Motion

In Section 3.5, we hypothesised that the velocity distributions should take Gaussian forms and, consequentially, the speed distribution should be that of a Rayleigh distribution. This conjecture was founded on the theory of Brownian motion. However, one may wish to assert that sea turtle movement is not congruent with that of a Brownian particle; animal trajectories are influenced by prey density, food scarcity, and predator abundance. In this section, we fit Speedy's velocity and speed empirical data to various statistical distributions with the aim of testing this hypothesis.

4.1 Fitting Distributions to the Data

To begin, we shall fit a Rayleigh distribution to the empirical speed data. In Figure 4.1, we notice that the Rayleigh distribution fits the data well for speeds less than 1.5 km/h, with some overestimation and underestimation by the Rayleigh fit at the crest of the histogram. Most notably, one may observe that the tail of the Rayleigh fit greatly overestimates the tail of the empirical data. There is also some noise present for speeds greater than 2.5 km/h,

likely due to the low volume of data remaining after filtering and cleaning.

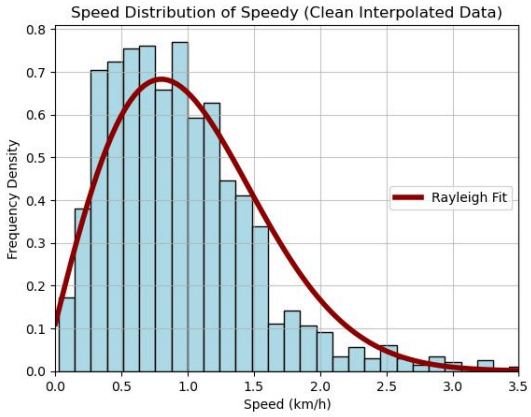

Figure 4.1: Cleaned, interpolated speed data fitted to a Rayleigh distribution (self-produced using Python; see Sections III and X).

In order to test our hypothesis further, we shall fit the x-velocity and y-velocity distributions to Gaussian distributions. From Figure 4.2, we observe that the Gaussians roughly fit the velocity distributions. There are large overestimations for low velocities (-0.5 km/h to 0.5 km/h), particularly for the x-velocity distribution.

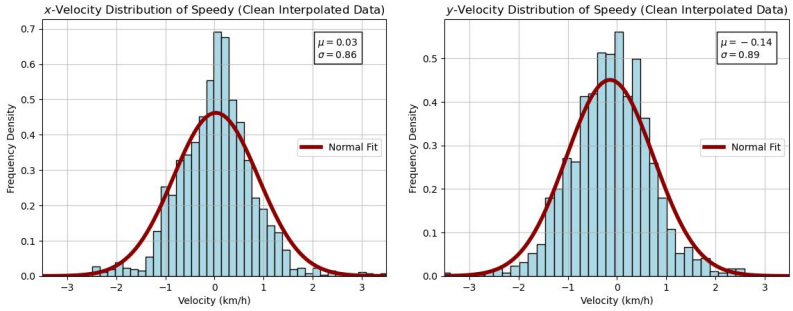

Figure 4.2: Cleaned, interpolated velocity data fitted to Gauss distributions (self-produced using Python; see Sections III and X).

Both Gaussians fit the x-velocity and y-velocity distributions well for intermediate velocities (0.5 km/h to 1.5 km/h, -1.5 km/h to -0.5km/h) with some noise present for larger velocities ($>$ 1.5 km/h, $<$ -1.5 km/h). The poor fit of the tails implies that further analysis of how the tails decay is required. We shall explore this in the next section.

4.2 Analysis of the Tails

To conduct this further analysis, we shall use semi-log plots and log-log plots to test how the tails of each empirical distribution decay. Semi-log plots are used to examine whether a given tail decays as an exponential [NW99]. This can be seen by first assuming the functional form of the tail is given by a general exponential:

$$y = e^{ax+b}, \text{ where } a, b \in \mathbb{R}$$

Then, plotting this assumed exponential tail against a logarithmic y-axis, whilst maintaining a linearly-scaled x-axis would transform the above exponential in the following way:

$$\begin{aligned} \ln(y) &= \ln\left(e^{ax+b}\right) \\ &= ax + b \end{aligned}$$

Thus, if the tail exponentially decays almost perfectly, the semi-log plot should reveal a linear relationship between x and $\ln(y)$ [NW99]. Figure 4.3 indicates that the tail begins to decay exponentially, but becomes erratic for larger speeds (>2.35 km/h). This may be a symptom of the low volume of cleaned data for such large speeds. One may also wish to check whether the tails decay as a power law. This can be done by plotting the tails on a log-log plot [KLV07]. If we assume the tail has the functional form of a power law:

$$y = bx^a, \text{ where } a, b \in \mathbb{R}$$

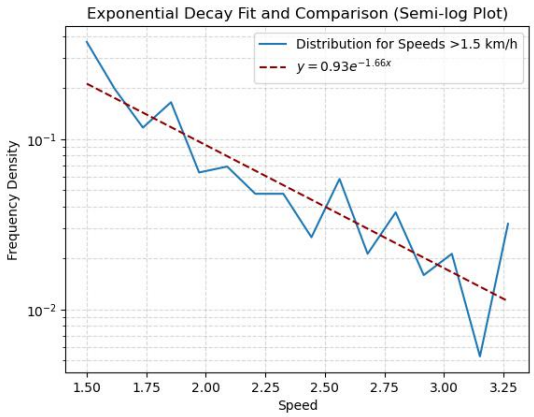

Figure 4.3: The right-tail (>1.5km/h) of the cleaned, interpolated speed distribution on a semi-log plot. The red dashed line illustrates the best exponential fit to the tail (self-produced using Python; see Sections III and XI of the accompanying Jupyter notebook).

Then, plotting this against logarithmic axes provides the following transformation:

$$\begin{aligned} \ln(y) &= \ln\left(bx^a\right) \\ &= a\ln(x) + \ln(b) \end{aligned}$$

Thus, if the tail decays in accordance with a power law, the semi-log plot should reveal a linear relationship between $\ln(x)$ and $\ln(y)$ [KLV07]. Figure 4.4 shows that the decay of the retail is more reminiscent of a power law, particularly for speeds less than 2.35 km/h. However, we also note that we have incompatibility with a power law fit for larger speeds. Again, this is likely due to the noise observed for larger speeds from the distribution (c.f. Figure 4.1). We shall now turn our attention to the semi-log and log-log plots of the x-velocity and y-velocity tails. Figure 4.5 further exemplifies the low volume of data for large values. However, according to the semi-log plot, the x-velocity and y-velocity seemingly decay exponentially. Moreover, one

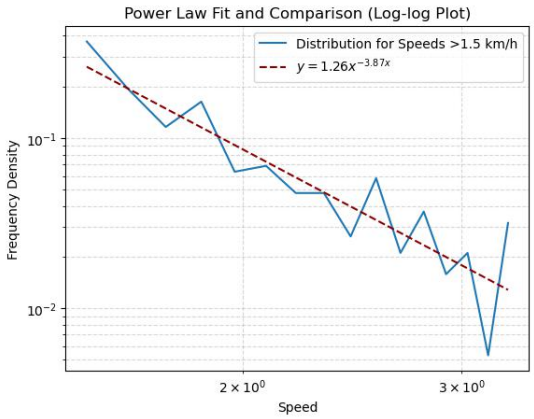

Figure 4.4: The right-tail (>1.5km/h) of the cleaned, interpolated speed distribution on a log-log plot (self-produced using Python; see Sections III and XI of the accompanying Jupyter notebook).

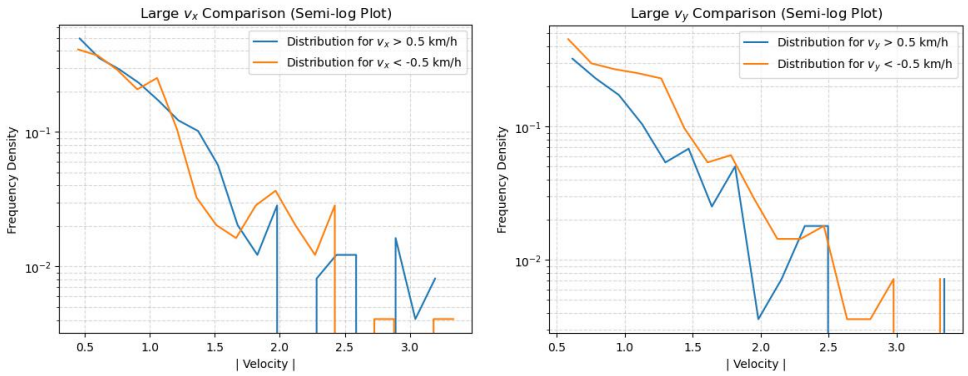

Figure 4.5: Semi-log plots of the x-velocity and y-velocity distribution tails (self-produced using Python; see Sections III and XI).

can observe the symmetry between the two tails of each distribution in this plot, indicating that symmetrical distributions are being portrayed for the velocities of Speedy.

Similarly, we can examine whether the tails of the velocity distributed decay

as a power law. Figure 4.6 shows that the tails of the velocity distributions certainly do not decay as a power law. However, the figure further demonstrates the symmetry between the tails of each distribution, bolstering the claim that the velocity distributions adopt a rough Gaussian form and furthering the plausibility of the hypothesis postulated in Section 3.5. Though

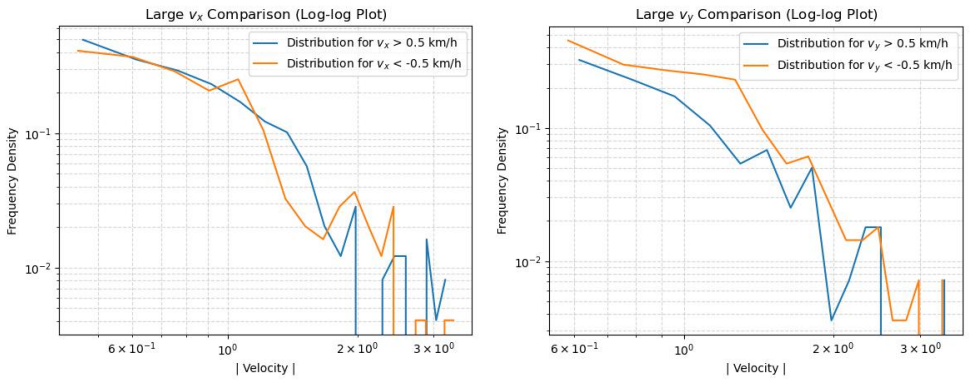

Figure 4.6: Log-log plots of the x-velocity and y-velocity distribution tails (self-produced using Python; see Sections III and XI).

simple fitting approaches, semi-log and log-log plots provide a rough indication as to whether the empirical data is aligned with a chosen distribution, we require a more explicit approach to test to what extent the empirical speed and velocity data correspond to various statistical distributions.

4.3 Quantile-Quantile Plots

Quantile-quantile plots allow statisticians to compare the distributions of two datasets [Mar04]. By plotting the quantiles of the empirical data against the quantiles of data sampled from a specific distribution, one can determine how well the empirical data fits the specific distribution in mind [AD18]. Furthermore, each of the quantile-quantile plots will be accompanied by a

coefficient of determination (R^2) calculation. The coefficient of determination is a quantifiable measure of how well an empirical dataset fits that of a given distribution [SRC12; Zha17]; an R^2 value closer to one implies a perfect fit, whereas an R^2 value closer to zero suggests a poor fit.

We begin by discussing Figure 4.7: the quantile-quantile plot of the speed dataset against a Rayleigh distribution. The solid red line indicates a perfect match between the two sets of quantiles. The closer the series of quantile-quantile points are to the solid red line, the better the empirical data aligns with the Rayleigh distribution. One can observe that the empirical speed data closely resembles that of Rayleigh-distributed data for speeds less than 1.75 km/h. This is somewhat consistent with Figure 4.1 and its related commentary; the Rayleigh distribution is an insufficient fit for the right-tail of the empirical speed data. Therefore, we may wish to test the fit of other distri-

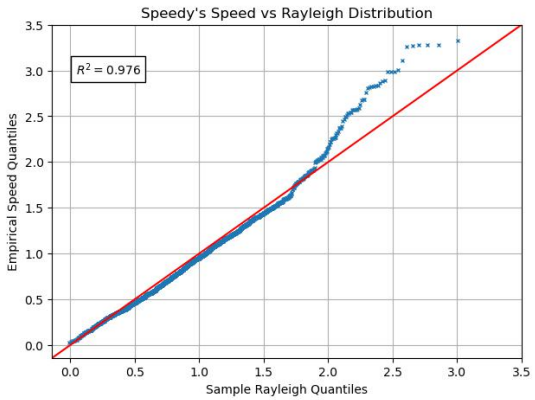

Figure 4.7: The quantile-quantile plot of the empirical speed quantiles against that of sampled Rayleigh-distributed data (self-produced using Python; see Sections III and XII of the accompanying Jupyter notebook).

butions that are related to modelling movement [San+20, Table 1]. Figure 4.8 compares the quantiles of the empirical speed data with that of data sampled from Gamma, Generalised Gamma, Log Gamma, and Weibull dis-

tributions. One may first notice that the Gamma distribution proves to be a better fit for the empirical speed data. We shall discuss this further in Section 4.5. Moreover, the Weibull, Gamma, and Generalised Gamma share similar

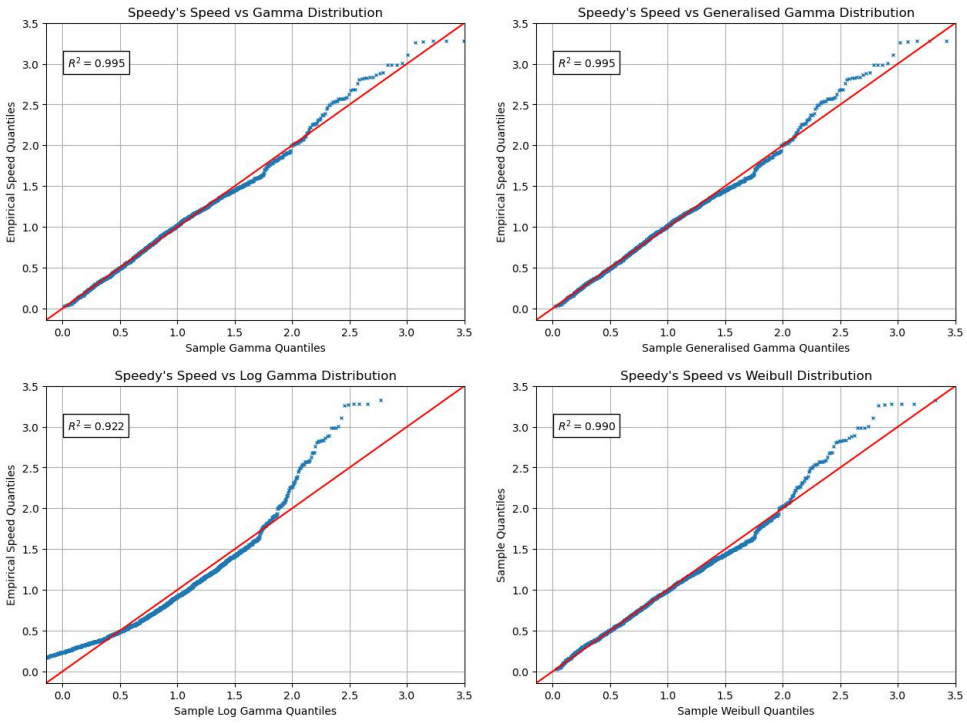

Figure 4.8: The quantile-quantile plot of the speed quantiles against that of data sampled from Gamma, Gen. Gamma, Log Gamma, and Weibull distributions (self-produced using Python; see Sections III and XII).

quantile-quantile plots. The Weibull and Gamma distributions share similar shapes for approximately equivalent respective parameter values. However, the Weibull distribution decays more quickly for large shape parameter values than the Gamma distribution which could be observed in their respective quantile-quantile plots. Unsurprisingly, the Gamma and Generalised Gamma distributions share similar shapes for set parameter values.

We shall now comment on the quantile-quantile plots for the x-velocity and

y-velocity distributions. Figure 4.9 illustrates the Gaussian-like behaviour of both velocity distributions, particularly for the y-velcoity of Speedy. However, in congruence with the previous commentary in Section 4.1, the tails of both velocity distributions do not align exactly with a Normal distribution. Therefore, it would be sensible to test the tails of the velocity distributions

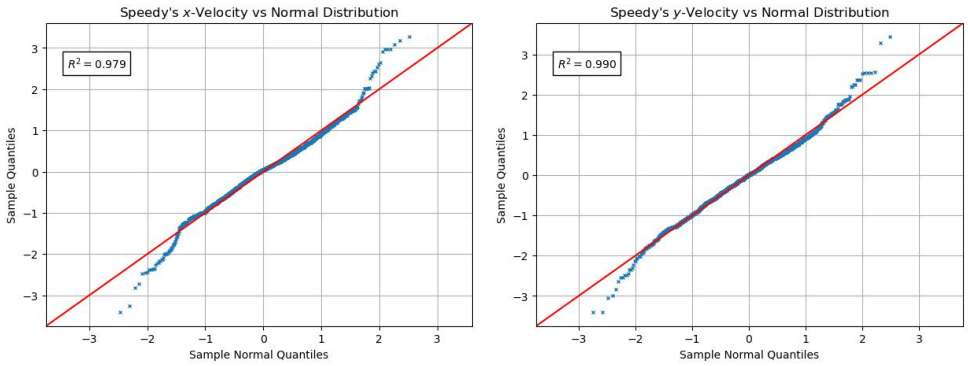

Figure 4.9: Quantile-quantile plots of the empirical x-velocity and y-velocity quantiles against that of Normal distributions (self-produced using Python; see Sections III and XII).

to determine the extent to which they align with exponential distributions or power law distributions. Figure 4.10 corroborates the behaviour observed in Figure 4.3; the quantile-quantile plots of the velocity tails illustrate the exponential decays of the velocity distributions. In addition, it can be shown via a quantile-quantile plot that the tails of the velocity distributions do not decay as a power law (see Figure F.1).

4.4 Calculating the Mean Square Displacement from the Empirical Data

In Section 2.4.2, we derived the mean square displacement (see Definition 2.1.3) from the Langevin equation and deduced that, for a Brownian parti-

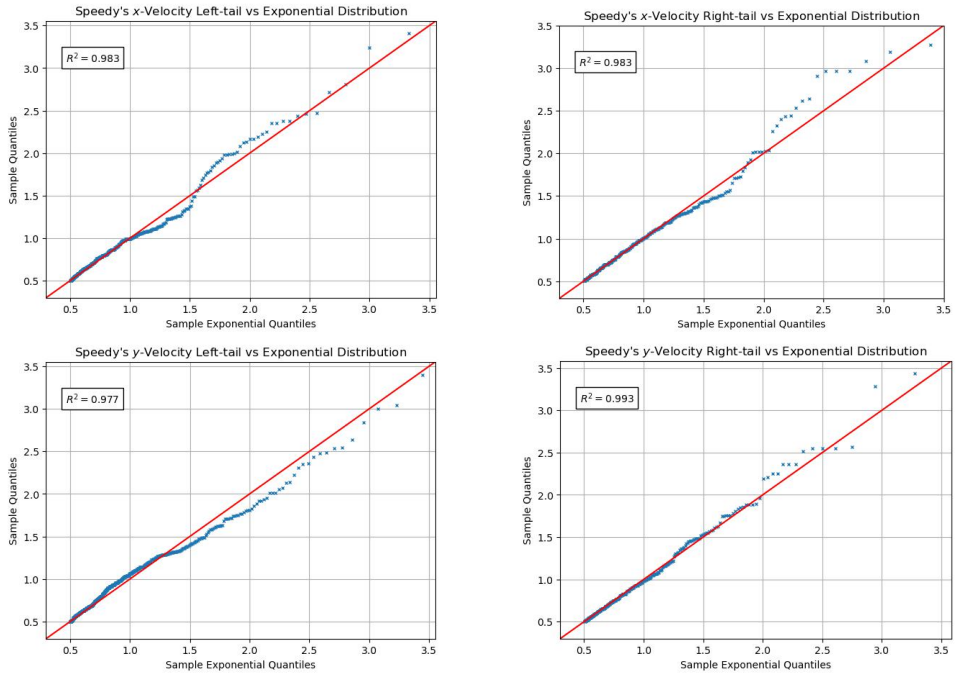

Figure 4.10: Quantile-quantile plots of the tails (>0.5 km/h; <-0.5 km/h) of the empirical x-velocity and y-velocity quantiles against that of exponential distributions (self-produced using Python; see Sections III and XII of the accompanying Jupyter notebook).

cle, the mean square displacement increases linearly in time. This is a key defining descriptor of Brownian motion. Thus, it would be sensible to test to what extent the mean square displacement of the turtle trajectories obey this linear growth over time.

Figure 4.11 shows that the mean square displacement for Speedy's trajectory does not strictly increase linearly with time and furthers the claim that the empirical data does not wholly align with the theory of Brownian motion.

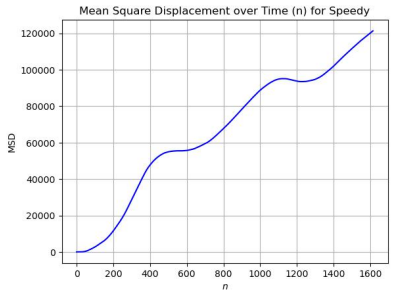

Figure 4.11: The mean square displacement for Speedy's raw interpolated trajectory (self-produced using Python; see Sections III and XV).

4.5 Evaluation

In our initial hypothesis, we assumed that the turtle movement would adhere to the theory of Brownian motion; the velocities would be Gaussian-distributed and the speed would be Rayleigh-distributed. The semi-log plots of the velocity tails (Figure 4.5), the simple fits of the velocity distributions themselves (Figure 4.2), and the simple fit of the Rayleigh distribution to the speed distribution (Figure 4.7) somewhat corroborate this hypothesis. However, we observed significant underestimations by the Gaussian fit for both velocities. Furthermore, the Gamma distribution proved to be a better fit than the Rayleigh distribution for the speed data (Figure 4.8; Figure G.1). Consequentially, one may assert that sea turtle movement does not adhere to the theory of Brownian motion; characteristics such as free will, sea conditions, and prey availability dictate the fluctuation of swimming speeds. Moreover, the large variance in time difference between GPS recordings, together with the linear interpolation, may have exacerbated the noise present within the dataset. This may have resulted in the Gamma distribution being a better fit for the speed data since the Gamma distribution is more flexible and can encapsulate such noise.

Chapter 5

Conclusions

This thesis sought to review the hierarchy of stochastic processes and apply it to empirical sea turtle movement data. By first defining the simple random walk, and illustrating how one can attain space- and time-continuity due to Donsker's Theorem, we explored how Wiener processes model space- and time-continuous movement. We then defined the Ornstein-Uhlenbeck process and provided motivation for the Langevin equation. By replicating a textbook derivation of the mean square displacement using the Langevin equation, we portrayed an important result of Brownian motion theory: the mean square displacement grows linearly with time. The theory discussed provided the foundations to present and process the empirical data.

The empirical data was cleaned and interpolated to be able to extract more precise functional forms from the velocity and speed distributions. We then used simple fits, semi-log plots, log-log plots, and quantile-quantile plots to test whether the velocity and speed distributions adhered to the theory of Brownian motion. Although the speed and velocity distributions somewhat conformed to Rayleigh and Gaussian distributions, the tails exhibitted significant regions of overestimation and underestimation throughout the plots.

This thesis has sufficiently shown that turtle movement does not strictly obey the theory of Brownian motion. One may postulate that the turtle's intrinsic needs, the environmental conditions of the sea, and prey density all impact the foraging patterns of the turtle; the movement of the sea turtle is more complex than that of a passive particle [Fre+18; Rev+07]. Whilst this manuscript has demonstrated that Brownian motion is insufficient to precisely model sea turtle foraging patterns, the question of whether there exists a holistic model of such motion remains to be answered. To this end, the theory of active, self-propelled Brownian particles [Bec+16] may be a suitable candidate for modelling the foraging movements of loggerhead sea turtles.

Bibliography

[Aba+23] S. Abalo-Morla et al. "Factors driving dispersal and habitat use of loggerhead sea turtle post-hatchlings and its conservational implications". In: *Marine Biology* 170.12 (Oct. 2023). ISSN: 1432-1793. DOI: 10.1007/s00227-023-04285-2. URL: http://dx.doi.org/10.1007/s00227-023-04285-2.

[Ada02] R. A. Adams. *Calculus*. 5th ed. Boston, MA: Addison Wesley, July 2002.

[AD18] A. Andersen and J. Dennison. "An introduction to quantile-quantile plots for the experimental physicist". In: *American Journal of Physics* 87.5 (2018).

[Arg24] Argos Services. *About Argos: Worldwide Satellite System — argos-system.org*. https://www.argos-system.org/about-argos/. [Accessed 30-07-2024]. 2024.

[AN05] S. Arora and E. Nabieva. "Markov Chains and Random Walks". In: (2005). URL: https://www.cs.princeton.edu/courses/archive/fall05/cos521/markov.pdf.

[Bat00] G. K. Batchelor. *Cambridge mathematical library: An introduction to fluid dynamics*. Cambridge, England: Cambridge University Press, Feb. 2000.

[Bec+16] C. Bechinger et al. "Active particles in complex and crowded environments". In: *Rev. Mod. Phys.* 88 (4 Nov. 2016), p. 045006. DOI: 10.1103/RevModPhys.88.045006. URL: https://link.aps.org/doi/10.1103/RevModPhys.88.045006.

[Ben16] E. Benson. "Movement Ecology and the Minimal Animal". In: *Interdisciplinary Journal of Landscape Architecture* 4 (2016), pp. 30–33.

[BW21] R. N. Bhattacharya and E. C. Waymire. *Random walk, brownian motion, and martingales*. Springer, 2021.

[Buc+20] G. M. Buchanan et al. "Assessment of national-level progress towards elements of the Aichi Biodiversity Targets". In: *Ecological Indicators* 116 (2020), p. 106497. ISSN: 1470-160X. DOI: https://doi.org/10.1016/j.ecolind.2020.106497. URL: https://www.sciencedirect.com/science/article/pii/S1470160X20304349.

[Cah+13] A. E. Cahill et al. "How does climate change cause extinction?" In: *Proceedings of the Royal Society B: Biological Sciences* 280.1750 (2013), p. 20121890. DOI: 10.1098/rspb.2012.1890. URL: https://royalsocietypublishing.org/doi/abs/10.1098/rspb.2012.1890.

[CS21] R. Chattamvelli and R. Shanmugam. "Rayleigh Distribution". In: *Continuous Distributions in Engineering and the Applied Sciences – Part II*. Cham: Springer International Publishing, 2021, pp. 245–252. ISBN: 978-3-031-02435-1. DOI: 10.1007/978-3-031-02435-1_9. URL: https://doi.org/10.1007/978-3-031-02435-1_9.

[CPB08] E. A. Codling, M. J. Plank, and S. Benhamou. "Random walk models in biology". In: *Journal of The Royal Society Interface* 5.25 (2008), pp. 813–834. DOI: 10.1098/rsif.2008.0014. URL:

https://royalsocietypublishing.org/doi/abs/10.1098/rsif.2008.0014.

[CKW04] W. T. Coffey, Y. P. Kalmykov, and J. T. Waldron. *The Langevin Equation*. 2nd. World Scientific, 2004. DOI: 10.1142/5343. URL: https://worldscientific.com/doi/abs/10.1142/5343.

[Con+21] O. Contreras-Vergara et al. "Langevin original approach and Ornstein–Uhlenbeck-type processes". In: *Physica A: Statistical Mechanics and its Applications* 584 (2021), p. 126349. ISSN: 0378-4371. DOI: https://doi.org/10.1016/j.physa.2021.126349. URL: https://www.sciencedirect.com/science/article/pii/S0378437121006221.

[Cri+92] T. O. Crist et al. "Animal Movement in Heterogeneous Landscapes: An Experiment with Eleodes Beetles in Shortgrass Prairie". In: *Functional Ecology* 6.5 (1992), pp. 536–544. ISSN: 02698463, 13652435. URL: http://www.jstor.org/stable/2390050 (visited on 06/20/2024).

[Cro04] M. Cross. *Langevin equation*. Feb. 2004. URL: http://www.pmaweb.caltech.edu/~mcc/Ph127/b/Lecture16.pdf.

[Cro23] M. Cross. *Physics 127b: Statistical Mechanics - Lecture 16*. Accessed: 2024-07-05. 2023. URL: http://www.pmaweb.caltech.edu/~mcc/Ph127/b/Lecture16.pdf.

[Csö79] M. Csörgő. "Brownian Motion—Wiener Process". In: *Canadian Mathematical Bulletin* 22.3 (1979), pp. 257–279. DOI: 10.4153/CMB-1979-033-1.

[Cus10] S. A. Cushman. *Animal movement data: GPS telemetry, autocorrelation and the need for path-level analysis*. Springer, 2010, pp. 131–149.

[DeA+21] D. L. DeAngelis et al. "Towards Building a Sustainable Future: Positioning Ecological Modelling for Impact in Ecosystems Management". In: *Bulletin of Mathematical Biology* 83.10 (2021), p. 107. DOI: 10.1007/s11538-021-00927-y.

[Don52] M. D. Donsker. "Justification and Extension of Doob's Heuristic Approach to the Kolmogorov- Smirnov Theorems". In: *The Annals of Mathematical Statistics* 23.2 (June 1952), pp. 277–281. ISSN: 0003-4851. DOI: 10.1214/aoms/1177729445. URL: http://dx.doi.org/10.1214/aoms/1177729445.

[Doo90] J. L. Doob. *Stochastic Processes*. en. Wiley Classics Library. Nashville, TN: John Wiley & Sons, Jan. 1990.

[Dur19] R. Durrett. "Markov Chains". In: *Probability: Theory and Examples*. Cambridge Series in Statistical and Probabilistic Mathematics. Cambridge University Press, 2019.

[Fre+18] C. Freitas et al. "Foraging behavior of juvenile loggerhead sea turtles in the open ocean: from Lévy exploration to area-restricted search". In: *Marine Ecology Progress Series* 595 (2018), pp. 203–215.

[GW14] E. T. Gilbert-Kawai and M. D. Wittenberg. "Reynold's number (and turbulent flow)". In: *Essential Equations for Anaesthesia: Key Clinical Concepts for the FRCA and EDA*. Cambridge University Press, 2014, pp. 21–23.

[Goi+21] T. Goicolea et al. "Deterministic, random, or in between? Inferring the randomness level of wildlife movements". In: *Movement Ecology* 9.1 (2021), p. 33. DOI: 10.1186/s40462-021-00273-7.

[Has16] U. Hassler. "Wiener Processes (WP)". In: *Stochastic Processes and Calculus: An Elementary Introduction with Applications*. Cham: Springer International Publishing, 2016, pp. 151–177. ISBN:

978-3-319-23428-1. DOI: 10.1007/978-3-319-23428-1_7. URL: https://doi.org/10.1007/978-3-319-23428-1_7.

[HL13] J. Hermans and B. Lentz. *Equilibria and Kinetics of Biological Macromolecules*. Wiley, Oct. 2013. ISBN: 9781118733639. DOI: 10.1002/9781118733639. URL: http://dx.doi.org/10.1002/9781118733639.

[HL11] J. Hizak and R. Logozar. "A Derivation of the Mean Absolute DIstance in One-Dimensional Random Walk". In: *Tehnički glasnik* 5 (July 2011), pp. 10–16.

[Hut17] B. Hutchinson. *The Conservation Status of Loggerhead Populations Worldwide — The State of the World's Sea Turtles — SWOT — seaturtlestatus.org*. https://www.seaturtlestatus.org/articles/2017/the-conservation-status-of-loggerhead-populations-worldwide. [Accessed 27-08-2024]. 2017.

[Jac96] M. Jacobsen. "Laplace and the origin of the Ornstein-Uhlenbeck process". In: *Bernoulli* 2.3 (1996), pp. 271–286. DOI: 10.3150/bj/1178291723. URL: https://doi.org/10.3150/bj/1178291723.

[Kap91] W. Kaplan. *Advanced Calculus*. en. 4th ed. Upper Saddle River, NJ: Pearson, Sept. 1991.

[KLV07] T. Karagiannis, J.-Y. Le Boudec, and M. Vojnović. "Power law and exponential decay of inter contact times between mobile devices". In: *Proceedings of the 13th Annual ACM International Conference on Mobile Computing and Networking*. MobiCom '07. Montréal, Québec, Canada: Association for Computing Machinery, 2007, pp. 183–194. ISBN: 9781595936813. DOI: 10.1145/1287853.1287875. URL: https://doi.org/10.1145/1287853.1287875.

[KS11] J. Klafter and I. M. Sokolov. *First Steps in Random Walks: From Tools to Applications*. Oxford University Press, Aug. 2011. ISBN: 9780199234868. DOI: 10.1093/acprof:oso/9780199234868.001.0001. URL: https://doi.org/10.1093/acprof:oso/9780199234868.001.0001.

[KSZ96] J. Klafter, M. F. Shlesinger, and G. Zumofen. "Beyond brownian motion". In: *Physics today* 49.2 (1996), pp. 33–39.

[LL10] G. F. Lawler and V. Limic. *Random walk: a modern introduction*. Vol. 123. Cambridge University Press, 2010.

[Lem02] D. S. Lemons. *An Introduction to Stochastic Processes in Physics*. The Johns Hopkins University Press, 2002.

[LG97] D. S. Lemons and A. Gythiel. "Paul Langevin's 1908 paper "On the Theory of Brownian Motion" ["Sur la théorie du mouvement brownien, " C. R. Acad. Sci. (Paris) 146, 530–533 (1908)]". In: *American Journal of Physics* 65.11 (Nov. 1997), pp. 1079–1081. ISSN: 1943-2909. DOI: 10.1119/1.18725. URL: http://dx.doi.org/10.1119/1.18725.

[LK19] A. Löffler and L. Kruschwitz. "Wiener's Construction of the Brownian Motion". In: *The Brownian Motion: A Rigorous but Gentle Introduction for Economists*. Cham: Springer International Publishing, 2019, pp. 87–101. ISBN: 978-3-030-20103-6. DOI: 10.1007/978-3-030-20103-6_6. URL: https://doi.org/10.1007/978-3-030-20103-6_6.

[Lyo14] A. Lyon. "Why are Normal Distributions Normal?" In: *The British Journal for the Philosophy of Science* 65.3 (2014), pp. 621–649. DOI: 10.1093/bjps/axs046. URL: https://doi.org/10.1093/bjps/axs046.

[Mar04] J. I. Marden. "Positions and QQ Plots". In: *Statistical Science* 19.4 (2004), pp. 606–614. ISSN: 08834237. URL: http://www.jstor.org/stable/4144431 (visited on 08/29/2024).

[Mar99] D. Marenduzzo. *14. The Langevin equation*. Lecture Note. 1999. URL: https://www2.ph.ed.ac.uk/~dmarendu/ASP/Section14.pdf.

[Mar11] M. Martelli. *Introduction to discrete dynamical systems and chaos*. John Wiley & Sons, 2011.

[MO14] J. Milton and T. Ohira. *Mathematics as a Laboratory Tool: Dynamics, Delays and Noise*. Springer New York, 2014. ISBN: 9781461490968. URL: https://books.google.co.uk/books?id=r-WPBAAAQBAJ.

[NW99] J. C. Nekola and P. S. White. "The distance decay of similarity in biogeography and ecology". In: *Journal of biogeography* 26.4 (1999), pp. 867–878.

[New99] I. Newton. *The Principia: Mathematical Principles of Natural Philosophy*. Trans. by I. B. Cohen and A. Whitman. Los Angeles: University of California Press, 1999.

[Øks98] B. Øksendal. *Stochastic Differential Equations: An Introduction with Applications*. 5th. Springer, 1998. URL: https://link.springer.com/book/10.1007/978-3-642-14394-6.

[Pat+22] J. Patino-Martinez et al. "Globally important refuge for the loggerhead sea turtle: Maio Island, Cabo Verde". In: *Oryx* 56.1 (2022), pp. 54–62.

[RW05] C. E. Rasmussen and C. K. I. Williams. *Gaussian processes for machine learning*. en. Adaptive Computation and Machine Learning series. London, England: MIT Press, Nov. 2005.

[Rei09] F. Reif. *Fundamentals of statistical and thermal physics*. en. Waveland Press, Jan. 2009.

[Rev+07] M. Revelles et al. "Habitat use by immature loggerhead sea turtles in the Algerian Basin (western Mediterranean): swimming behaviour, seasonality and dispersal pattern". In: *Marine Biology* 151.4 (Jan. 2007), pp. 1501–1515. ISSN: 1432-1793. DOI: 10.1007/s00227-006-0602-z. URL: http://dx.doi.org/10.1007/s00227-006-0602-z.

[Rév13] P. Révész. *Random walk in random and non-random environments*. World Scientific, 2013.

[Rob04] J. C. Robinson. "Inhomogeneous second order linear equations". In: *An Introduction to Ordinary Differential Equations*. Cambridge University Press, 2004, pp. 131–140.

[Rom22] P. Roman Torres. "Environmental variation shapes life history traits of sea turtles: an ecological modelling approach". PhD thesis. Queen Mary, University of London, 2022.

[Ros10] S. M. Ross. "Chapter 10 - Brownian Motion and Stationary Processes". In: *Introduction to Probability Models (Tenth Edition)*. Ed. by S. M. Ross. Tenth Edition. Boston: Academic Press, 2010, pp. 631–666. ISBN: 978-0-12-375686-2. DOI: https://doi.org/10.1016/B978-0-12-375686-2.00012-1. URL: https://www.sciencedirect.com/science/article/pii/B9780123756862000121.

[Saj08] G. Sajeevan. "Latitude and longitude–A misunderstanding." In: *Current Science* 94.5 (2008).

[ST19] T. Sandev and Ž. Tomovski. "Generalized Langevin Equation". In: *Fractional Equations and Models: Theory and Applications*. Cham: Springer International Publishing, 2019, pp. 247–300. ISBN: 978-3-030-29614-8. DOI: 10.1007/978-3-030-29614-8_6. URL: https://doi.org/10.1007/978-3-030-29614-8_6.

[San+20] J. V. Santana-Filho et al. "A Langevin dynamics approach to the distribution of animal move lengths". In: *Journal of Statistical Mechanics: Theory and Experiment* 2020 (2020). URL: https://api.semanticscholar.org/CorpusID:213214221.

[SRC12] L. J. Saunders, R. A. Russell, and D. P. Crabb. "The Coefficient of Determination: What Determines a Useful R 2 Statistic?" In: *Investigative Ophthalmology Visual Science* 53.11 (Oct. 2012), pp. 6830–6832. ISSN: 1552-5783. DOI: 10.1167/iovs.12-10598. URL: https://doi.org/10.1167/iovs.12-10598.

[Sec01] Secretariat of the Convention on Biological Diversity. *Handbook of the convention on biological diversity*. Routledge, 2001. DOI: https://doi.org/10.4324/9781315071770.

[Sjo09] L. Sjogren. Feb. 2009. URL: http://gu-statphys.org/media/mydocs/LennartSjogren/kap6.pdf.

[SG96] W. Smith and M. Gillan. "The Random Walk and the Mean Squared Displacement". In: *Information Quarterly for Computer Simulation of Condensed Phases* (1996), pp. 54–64.

[Sto09] G. G. Stokes. "On the Effect of the Internal Friction of Fluids on the Motion of Pendulums". In: *Mathematical and Physical Papers*. Cambridge Library Collection - Mathematics. Cambridge University Press, 2009, pp. 1–10.

[TM03] S. T. Thornton and J. B. Marion. *Classical dynamics of particles and systems*. en. 5th ed. Florence, KY: Brooks/Cole, July 2003.

[Zha17] D. Zhang. "A coefficient of determination for generalized linear models". In: *The American Statistician* 71.4 (2017), pp. 310–316.

For references related to the coding element of this thesis, please see Section XVI of the accompanying Jupyter notebook.

Appendix A

Simulations of Stochastic Processes

In this section, one can see simulations of the various stochastic processes discussed throughout Chapter 2.

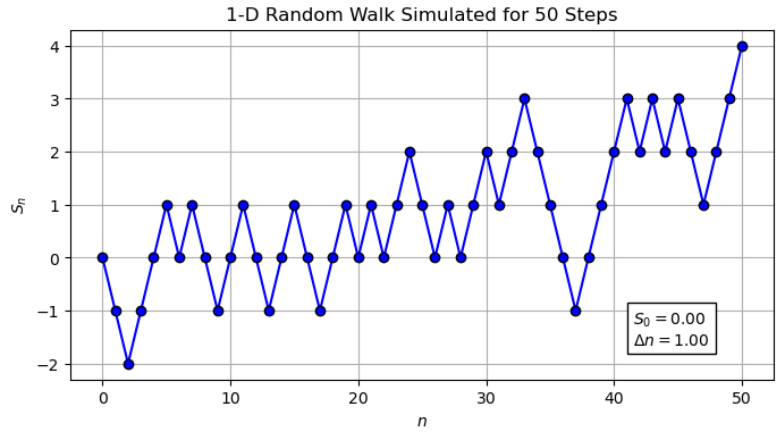

Figure A.1: This is an example of a random walk (see Definition 2.1.1). The walker starts at the origin and performs fifty steps: $X_1 = -1$; $X_2 = -1$; ...; $X_{50} = 1$. The overall displacement of the walk from the origin is given by S_{50} (self-produced using Python; see Section II).

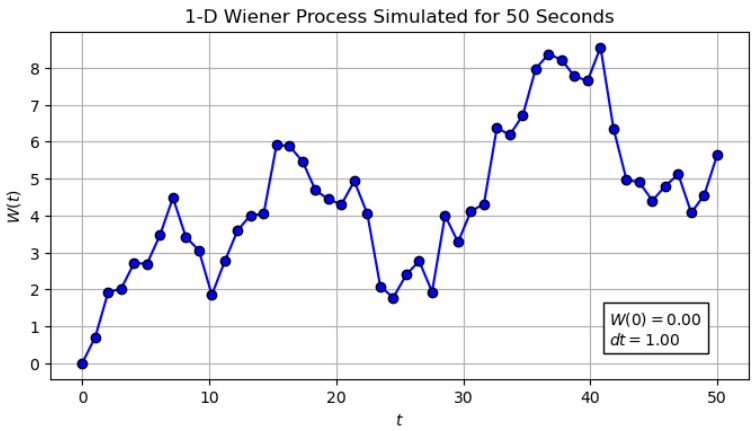

Figure A.2: A one-dimensional Wiener process (see Definition 2.2.1) running for fifty seconds. One can observe that the process starts at zero and that the increments are not of equal length (self-produced using Python; see Section II of the accompanying Jupyter notebook).

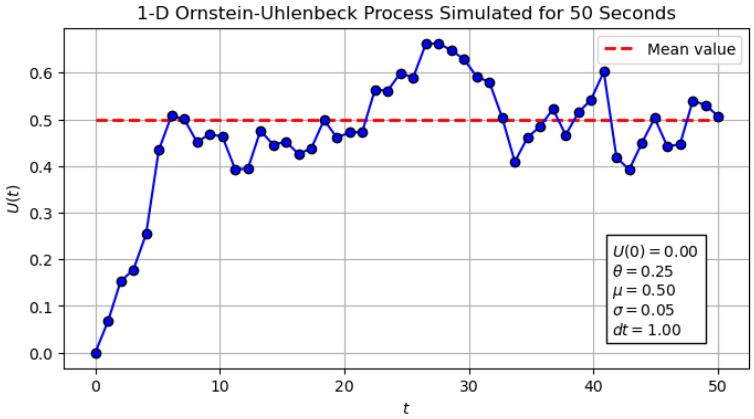

Figure A.3: A one-dimensional Ornstein-Uhlenbeck process (see Definition 2.3.1) running for fifty seconds. One can observe the mean reversion property, noting that the walker lingers around the mean value (self-produced using Python; see Section II).

Appendix B

Gaussian Tendency of the Position Distribution

Please click the link here to see an animation illustrating the Gaussian tendency of the position distribution of a random walk. The animation is a frame-by-frame GIF showing the distribution for increasing integer values of n such that $0 \leq n \leq 10$ (self-produced using Python; see Section II of the accompanying Jupyter notebook).

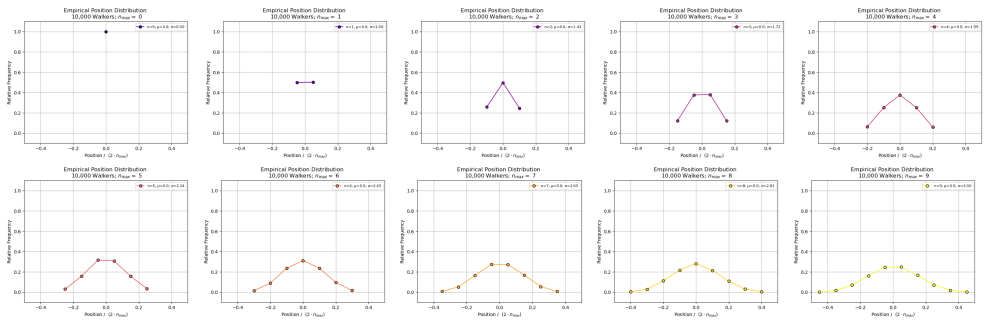

Figure B.1: The first ten frames of the animation (self-produced using Python; see Section II of the accompanying Jupyter notebook).

Appendix C

A Physical Derivation of the Langevin Equation

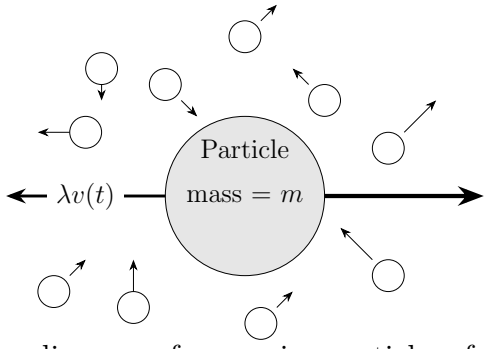

Figure C.1: A force diagram of a massive particle, of mass m, moving in a viscous fluid, of viscosity coefficient λ, illustrating the noise-generating forces from the surrounding particles (self-produced, using TikZ).

In this section, we aim to illustrate the Langevin equation of motion (see Definition 2.4.1) using elementary Newtonian mechanics and Stokes' Law ([Bat00]; see also [Sto09]). In 1908, Paul Langevin stated a differential equation to describe the empirically observed motion of a large particle in a viscous fluid. The physicist began by recognising that the resultant force acting on

the particle is governed by Newton's Second Law ([TM03]; see also [New99]) and that Stoke's Law [Sto09] describes the friction force applied to a large particle in a fluid with viscosity coefficient λ. If these two terms are the only constituting factors of the motion, then the particle would eventually become stationary (see Equation C.1).

$$m\frac{\mathrm{d}v(t)}{\mathrm{d}t} = -\lambda v(t) \tag{C.1}$$

Langevin recongised this; he introduced a "complementary force", $\xi(t)$, which accounts for the agitations that can be observed in such motion [LG97]. Thus, the equation of motion becomes:

$$\begin{aligned} m\frac{\mathrm{d}v(t)}{\mathrm{d}t} &= -\lambda v(t) + \xi(t) \\ \Rightarrow \quad \frac{\mathrm{d}v(t)}{\mathrm{d}t} &= -\frac{1}{m}\lambda v(t) + \frac{1}{m}\xi(t) \end{aligned} \tag{C.2}$$

Therefore, the Langevin equation of motion (Equation C.2, cf. Definition 2.4.1) describes the movement of a particle within a fluid of viscosity coefficient λ, synthesising both deterministic and probabilistic forces.

Appendix D

Latitude-Longitude Plot for the Foraging Period

Figure D.1 illustrates the latitude-longitude plot for the sea turtles during their foraging period. As mentioned in Section 3.2, the foraging period commences for each turtle after each turtle's first sharp turn.

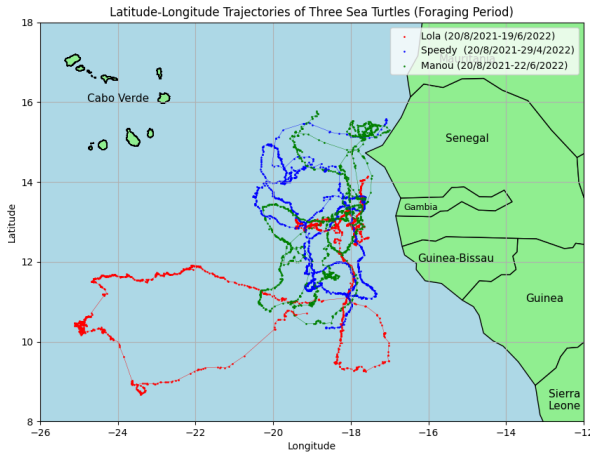

Figure D.1: The latitude-longitude during the foraging periods for Lola, Manou, and Speedy (self-produced using Python; see Sections III and IV of the accompanying Jupyter notebook).

Appendix E

Speed Throughout the Foraging Period

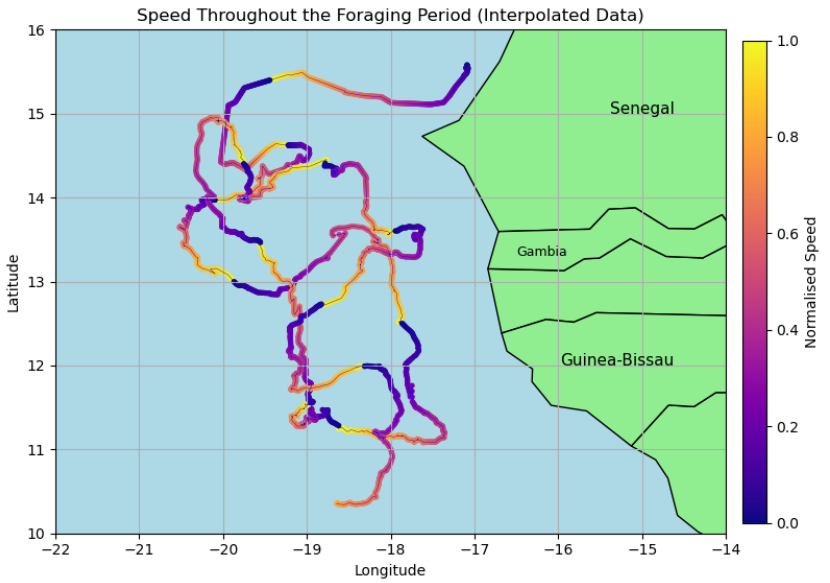

Figure E.1: The normalised speed throughout Speedy's foraging period indicated as a colour-map (self-produced using Python; see Sections III and XIV of the accompanying Jupyter notebook).

Appendix F

Q-Q Plots: x-Velocity, y-Velocity vs. Power Law

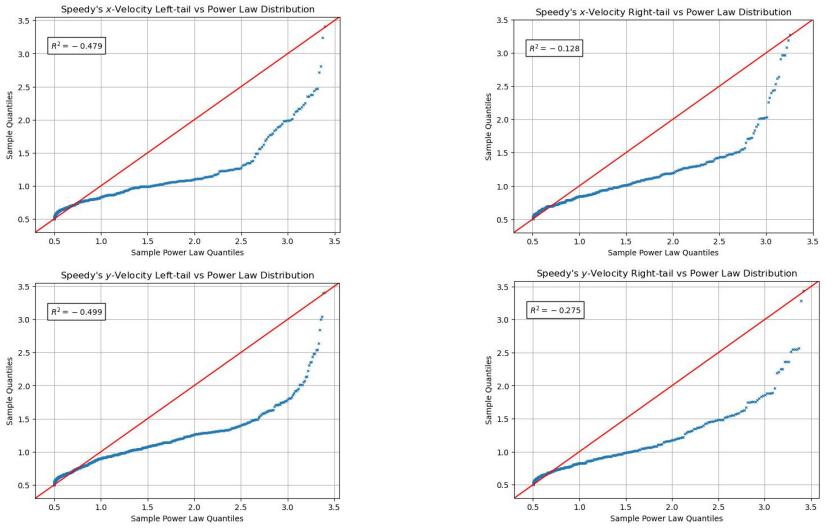

Figure F.1: Quantile-quantile plots of the tails (>0.5 km/h; <-0.5 km/h) of the empirical x-velocity and y-velocity quantiles against that of power law distributions. The absolute value of the left tail has been taken to compare symmetry between the two tails (self-produced using Python; see Sections III and XII of the accompanying Jupyter notebook).

Appendix G

Simple Fit: Gamma Distribution to Speed

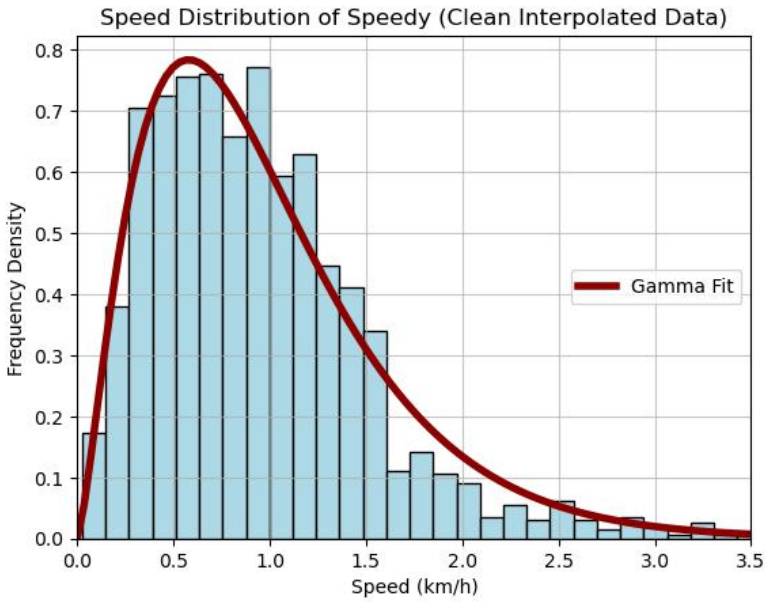

Figure G.1: Cleaned, interpolated speed data fitted to a Gamma distribution (self-produced using Python; see Sections III and X).